Characterizing High Frequency Gravity Wave Propagation Through an Evolving Inertial Wave in the MLT

Email: tyler@gats-inc.com

Tyler Mixa[1,2], Katrina Bossert[1], Dave Fritts[1], Brian Laughman[1], Tom Lund[3], Lakshmi Kantha[2]

[1]Global Atmospheric Technologies and Sciences (GATS)-inc, Boulder, CO, USA
[2]University of Colorado Boulder, Boulder, CO, USA
[3]Northwest Research Associates (NWRA), Boulder, CO, USA

MLTG-06
Mesosphere and Lower Thermosphere Gravity Waves

Introduction

On 21 January 2015, a sodium resonance lidar and advanced mesospheric temperature mapper (AMTM) observed intermittent propagation of a high frequency gravity wave (HFGW) through an inertial gravity wave (IGW) over Alomar, Norway. The evolving IGW can promote critical layers, reflection, evanescence, and tunneling as the HFGW propagates through alternating IGW phases. A high resolution anelastic numerical model is used to characterize the HFGW propagating through the IGW and account for the temporal variability in the observational data.

Methodology and Objectives

- Initialize HFGW with observed characteristics and propagate into lidar wind and temperature profiles
- Assess GW behavior for most likely λ_z, ω_i, and amplitude
- Evaluate GW source intermittency and turbulence source
- Address discrepancies in amplitudes and intermittency between AMTM and lidar observations

Simulation Architecture

- 3D, anelastic, nonlinear, finite volume DNS
- Conserves mass, momentum, & kinetic energy
- Can resolve dissipation scales in the MLT
- Density scales with altitude

Architecture-Specific Definitions

$$\frac{\theta'}{\overline{\theta}} = -\frac{\rho'}{\overline{\rho}} + \frac{p'}{\overline{\rho} g H} \qquad \mu = \mu_0 \frac{T_0 + c}{T + c}\left(\frac{T}{T_0}\right)^{\frac{3}{2}}$$

$$\frac{T'}{\overline{T}} = \frac{p'}{\overline{p}} - \frac{\rho'}{\overline{\rho}} = \frac{\theta'}{\overline{\theta}} + \frac{p'}{\overline{p}}\left(1 - \frac{\overline{p}}{\overline{\rho} g H}\right)$$

Solution variables (u_i, θ, p')

$$\frac{\partial \overline{\rho} u_j}{\partial x_j} = 0$$

$$\frac{\partial \overline{\rho} u_i}{\partial t} + \frac{\partial \overline{\rho} u_i u_j}{\partial x_j} = -\frac{\partial p'}{\partial x_i} + \left(\frac{\overline{\rho}\theta' g}{\overline{\theta}} - \frac{p'}{H}\right)\delta_{i3} + \frac{\partial}{\partial x_j}\left[\mu\left(\frac{\partial u_i}{\partial x_j} + \frac{\partial u_j}{\partial x_i}\right)\right]$$

$$\frac{\partial \overline{\rho}\theta}{\partial t} + \frac{\partial \overline{\rho}\theta u_j}{\partial x_j} = \frac{\overline{\theta}}{c_p \overline{T}}\left[\mu\left(\frac{\partial u_i}{\partial x_j} + \frac{\partial u_j}{\partial x_i}\right)\frac{\partial u_i}{\partial x_j} - \frac{\partial}{\partial x_j}\left(\kappa \frac{\partial T}{\partial x_j}\right)\right]$$

Guiding Observations

AMTM Overview of HFGW Characteristics:

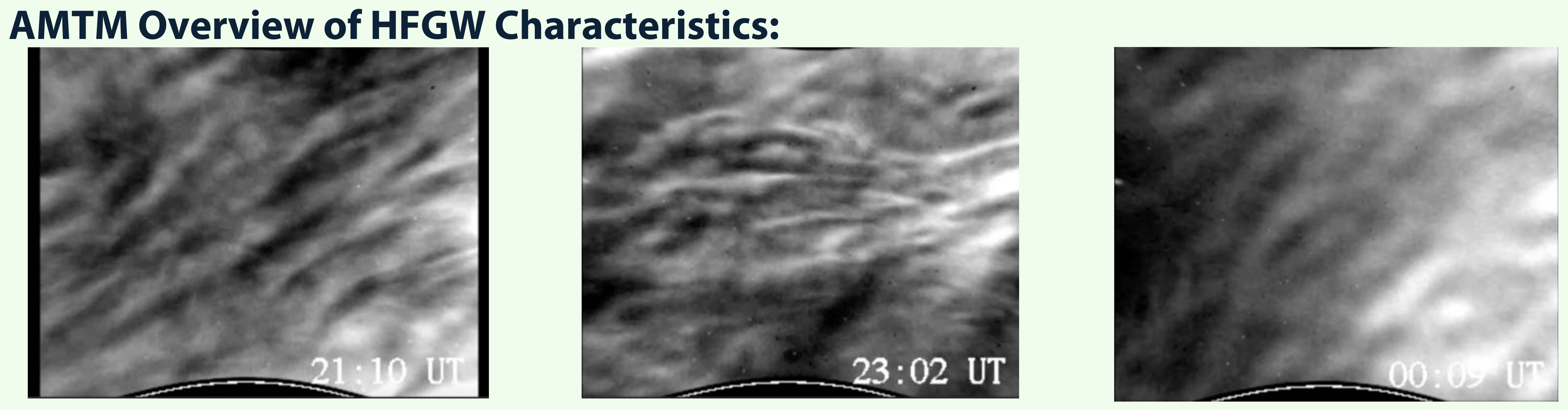

Same apparent HFGW at 21 UT and 24-25 UT with instabilities at 22-23 UT

Lidar Overview of Background Environment and IGW Characteristics:

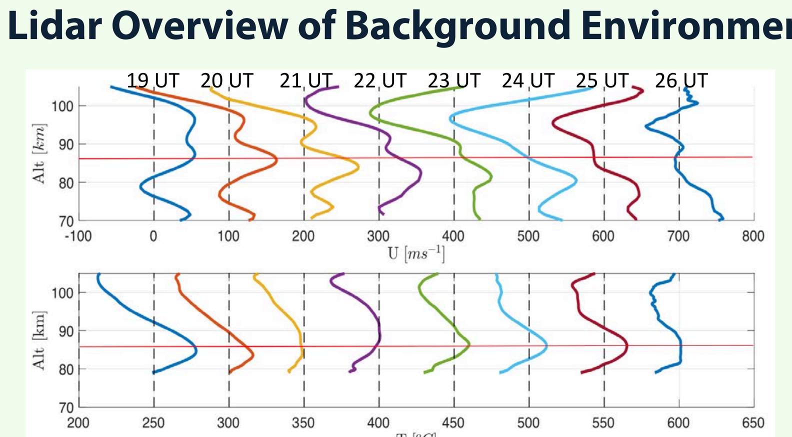

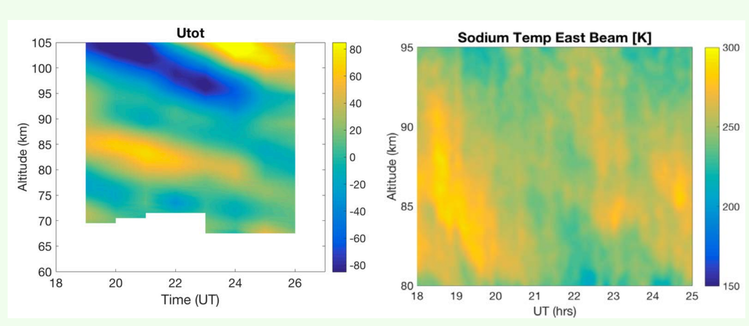

Background winds and temperatures include ~7 hour IGW, many higher frequency components

Observed GW Characteristics

HFGW Parameters from 21 UT AMTM Observation:

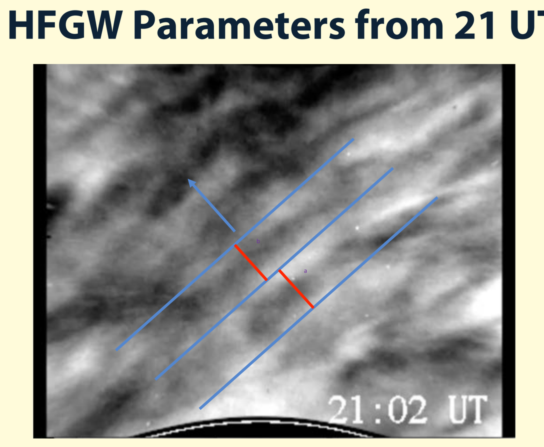

λ_x = 19-20km, c_o = 15 m/s
NW Propagation

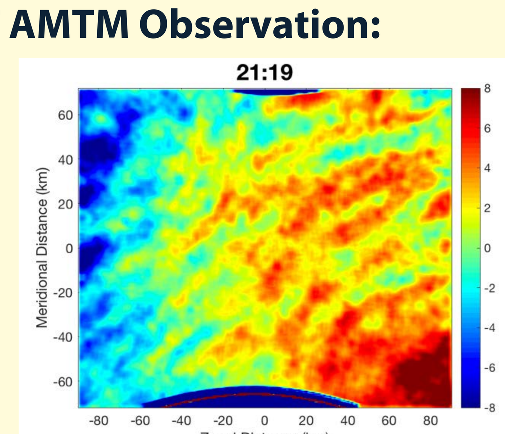

T' = ± 3K

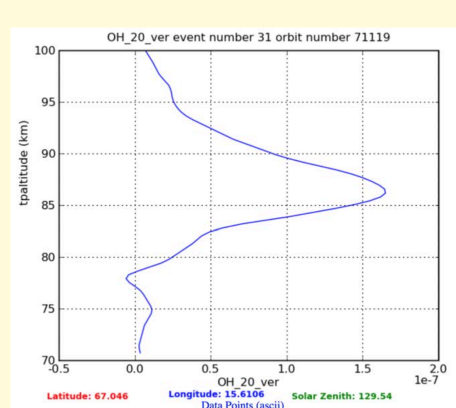

SABRE OH layer altitude: 86km

HFGW Parameters from Lidar Observation:

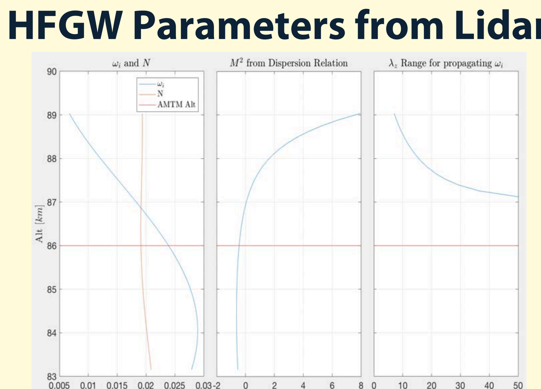

ω_i range: 0.008-0.016 s^{-1}
λ_z range: 8-28km

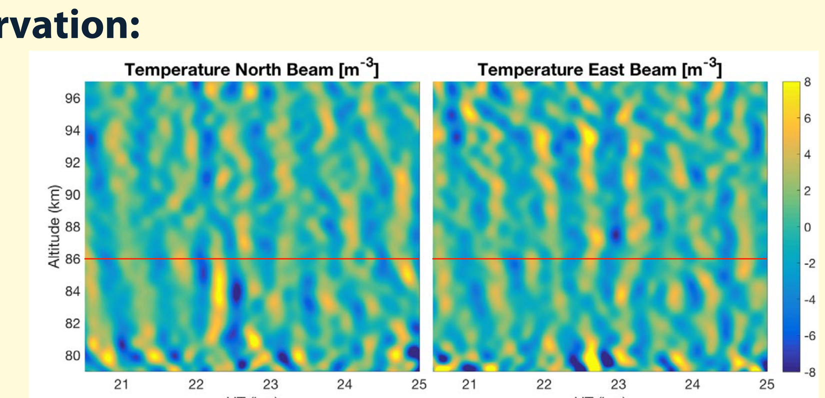

20-30 min period consistent with AMTM
Phase structures appear to have evanescent regions
T' = ± 10K at 80km, reduced amplitude at AMTM

Simulated GW Propagation through Observed Profiles

19-20 UT: Filtering

- Critical layer filtering at 80km
- Partial energy transmission into evanescent region at later times
- Scattered turbulence but no wave visible in AMTM
- Simulation data agrees with lidar and AMTM observations

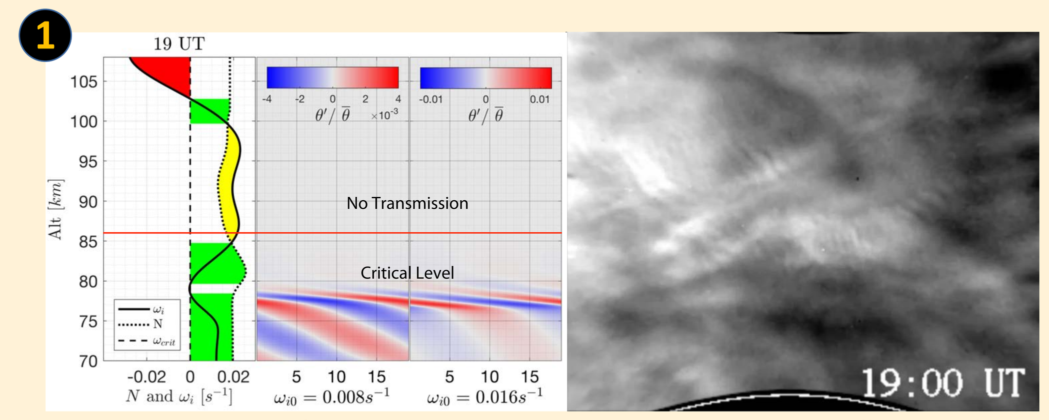

ω_i regimes at 19 UT showing propagation (green), evanescence (yellow), and ω_i < 0 (red); θ' fields from simulation showing no GW transmission through critical level; and AMTM intensity.

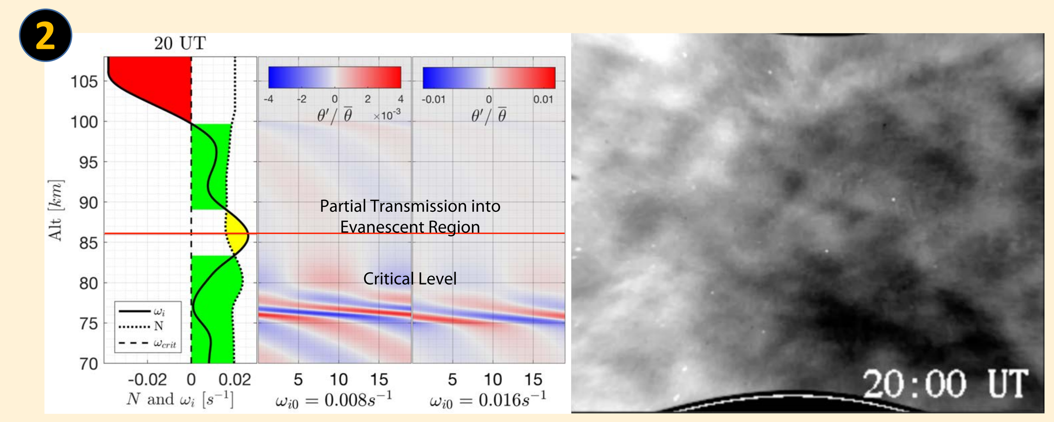

As in Figure 1 for 20 UT. θ' fields from simulation indicate partial transmission of wave energy through critical level at later times, with no coherent GW phase structure visible in AMTM.

21 UT: Propagation

- Coherent HFGW observed in AMTM
- Simulations show GW tunneling through evanescent region at AMTM altitudes
- Phase structure in lidar observations matches simulation outputs
- Lower T' amplitude in AMTM shown by lidar in evanescent region

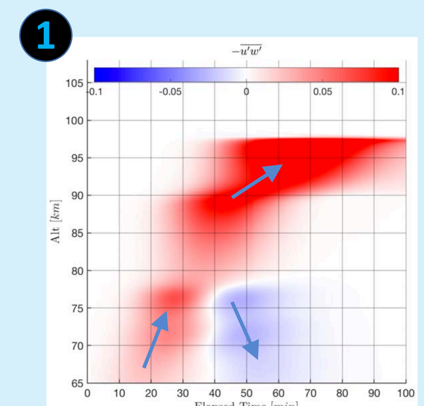

GW momentum flux indicates tunneling and reflection at evanescent layer.

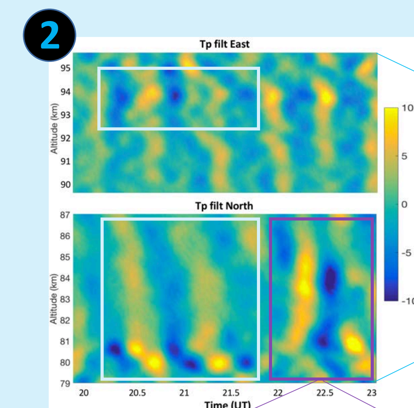

30 min filtered lidar temperatures show phase structure that matches simulations.

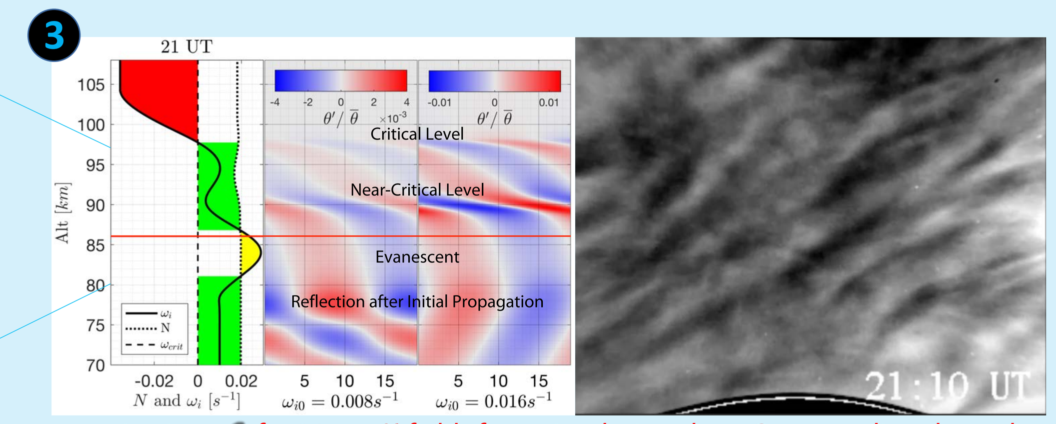

As in Figure 1 for 21 UT. θ' fields from simulation show GW tunneling through evanescent region at AMTM altitudes, with phase structure showing propagation above and below the evanescent region.

22-23 UT: Instabilities

- Instability features advect to the east through AMTM and do not align with wave vector or GW phases
- Simulations show potential for weak instability formation with higher ω_{i0} as shear and convective instability conditions develop at 85km
- Instabilities in simulations do not explain multiple scales and orientations of instabilities observed in AMTM

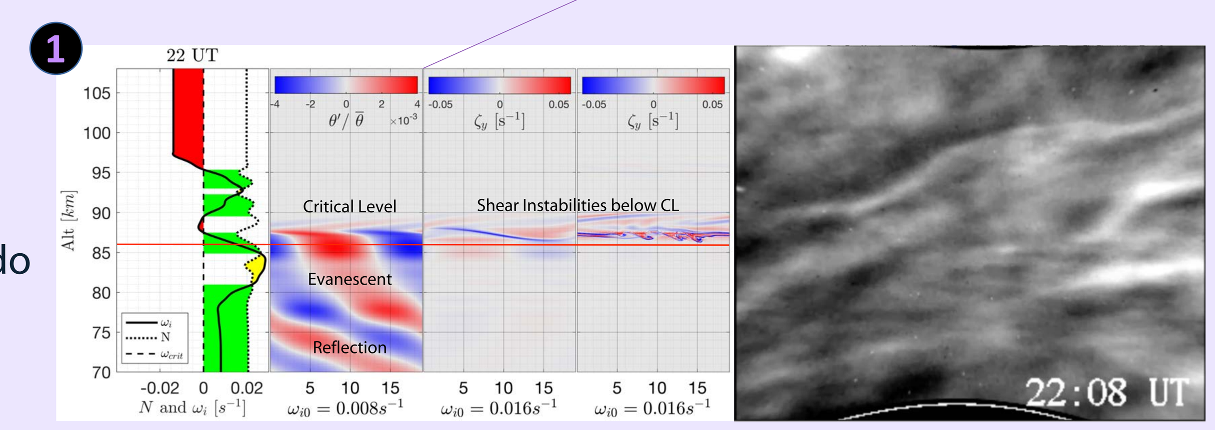

As in Figure 1 for 22 UT. θ' fields from simulation indicate critical level below 90km, while vorticity (ζ_y) shows potential for shear instability formation at later times with larger initial ω_i. Obscured GW in AMTM indicates instability formation.

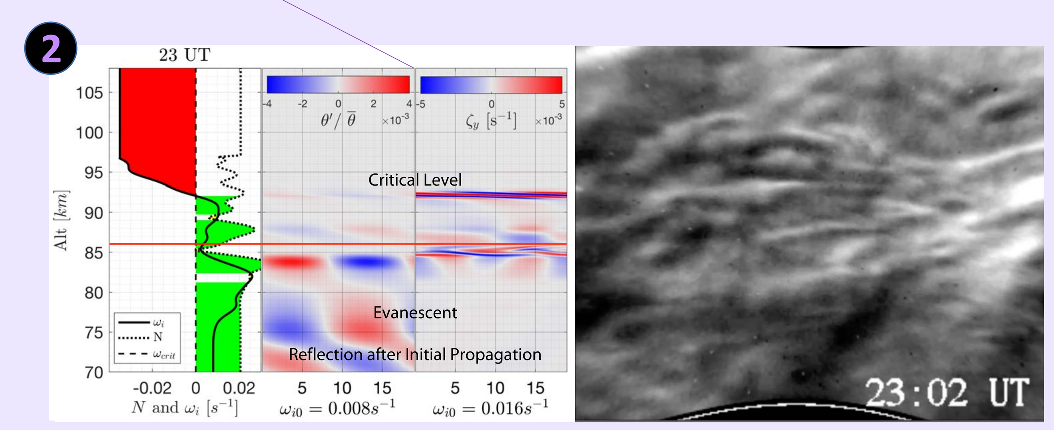

As in Figure 1 for 23 UT. AMTM intensity shows EW-aligned instabilities at at 86km where lidar has heightened T' amplitudes. θ' fields from simulation show potential for instability development at 86km where $N^2 < 0$.

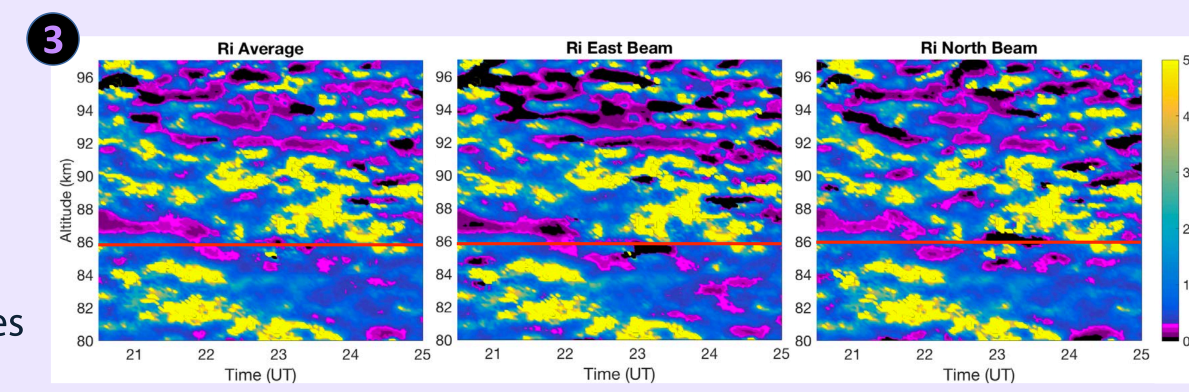

Ri from lidar winds and temperatures, showing convective and shear instability tendency from 21-23 UT. That convective Ri occurs at different altitudes in East and North beams suggests horizontally localized instability conditions that do not cover entire AMTM domain.

Instability Source

- Background Ri shows regions of convective and shear instability conditions from 21-23 UT
- Altitude discrepancy between negative Ri regions suggests horizontally localized instability conditions
- Simulations show potential for shear turbulence at 86km, but alignment and propagation of AMTM instabilities suggests advection through AMTM domain rather than GW generation

24-25 UT: Propagation

- GW observed in AMTM with same parameters as 21 UT
- Widening critical layer region reduces amplitude over time
- Similarity to HFGW observed at 21 UT suggests continuous wave source from 21-25 UT

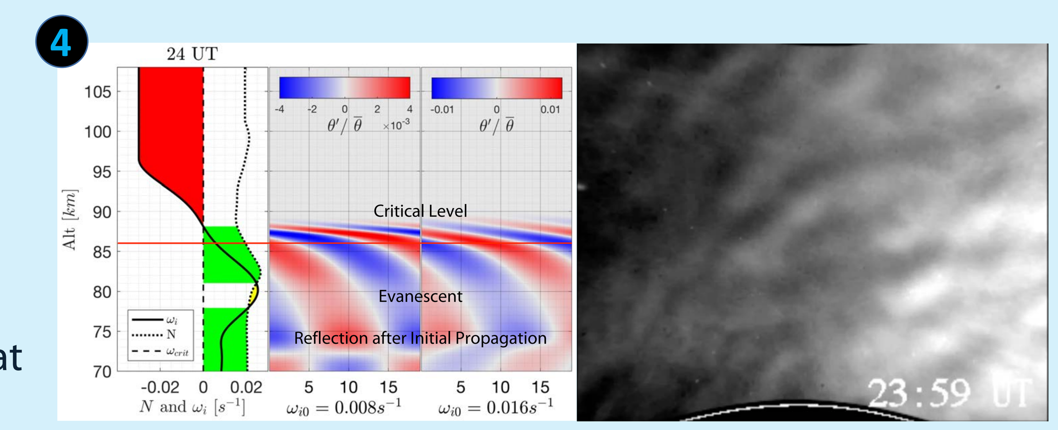

As in Figure 1 for 24 UT. θ' fields from simulation indicate propagation up to critical level above OH layer where wave is visible in AMTM. Wave characteristics in AMTM match observations from 21 UT.

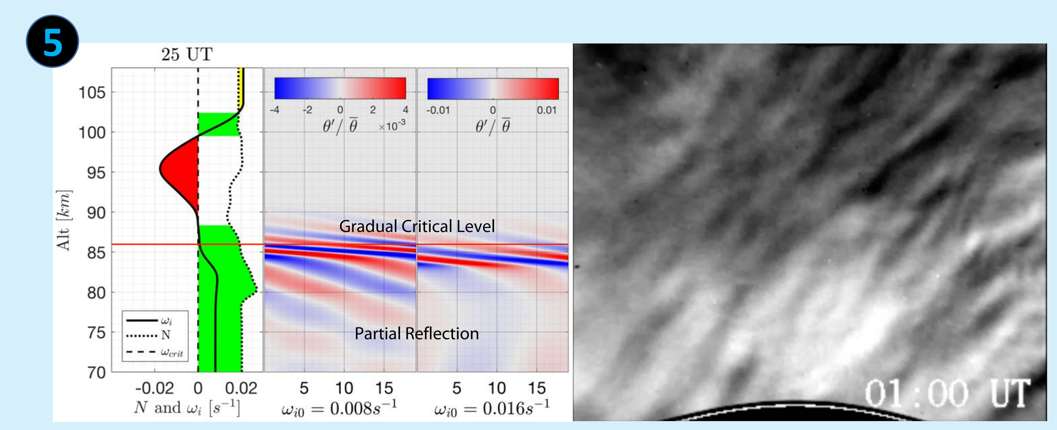

As in Figure 1 for 25 UT. Expanding critical level reduces θ' amplitude at AMTM altitudes. AMTM intensity shows wave signature slowly diminishing.

Conclusions

- Complex IGW environment provides unique opportunity to observe transient, propagating GW events in the MLT
- Intermittent HFGW event simultaneously observed by lidar and AMTM
- IGW background creates regions of reflection, propagation, evanescence/tunneling, and critical level filtering that account for amplitude variations in lidar and AMTM
- Observed instabilities in AMTM coincide with shear and convective instability conditions in Ri profiles, but GW is likely obscured by, rather than responsible for, instabilities in AMTM domain while propagation continues

Acknowledgments

AMTM and lidar data and analysis:
Katrina Bossert, P.D. Pautet, Mike Taylor
Additional support of this study:
Dave, Brian, and other GATS coworkers
Simulations run on DoD supercomputers
Research funding provided by the National Science Foundation

In loving memory of our friend and colleague, Brian Laughman 1979-2018